

S. Abdul Gaffar*, V. Ramachandra Prasad, P. Ramesh Reddy, and B.Md. Hidayathulla Khan

Radiative Flow of Third Grade Non-Newtonian Fluid From A Horizontal Circular Cylinder

<https://doi.org/10.1515/nleng-2018-0078>

Received May 19, 2018; revised November 11, 2018; accepted November 16, 2018.

Abstract: In this article, we study the nonlinear steady thermal convection of an incompressible third-grade non-Newtonian fluid from a horizontal circular cylinder. The transformed conservation equations are solved numerically subject to physically appropriate boundary conditions using a second-order accurate implicit finite-differences Keller Box technique. The influence of a number of emerging non-dimensional parameters, namely the third-grade fluid parameter (ϕ), the material fluid parameters (ϵ_1, ϵ_2), Prandtl number (Pr), Biot number (γ), thermal radiation (F) and dimensionless tangential coordinate (ξ) on velocity and temperature evolution in the boundary layer regime are examined in detail. Furthermore, the effects of these parameters on *surface heat transfer rate* and *local skin friction* are also investigated. Validation with earlier *Newtonian* studies is presented and excellent correlation is achieved. It is found that the velocity, skin friction and Nusselt number (heat transfer rate) reduce with increasing third grade fluid parameter (ϕ), whereas the temperature is enhanced. Increasing material fluid parameter (ϵ_1) reduces the velocity and heat transfer rate but enhances the temperature and skin friction. The study is relevant to chemical materials processing applications and low density polymer materials processing.

Keywords: Non-Newtonian Third-grade fluid, Material fluid parameters, Thermal Radiation, Biot number

*Corresponding Author: S. Abdul Gaffar, Department of Information Technology, Mathematics Section, Salalah College of Technology, Salalah, Oman, E-mail: abdulgaffar0905@gmail.com

V. Ramachandra Prasad, Department of Mathematics, School of Advanced Sciences, Vellore Institute of Technology, Vellore – 6322014, India

P. Ramesh Reddy, Department of Mathematics, Madanapalle Institute of Technology and Science, Madanapalle- 517325, India

B.Md. Hidayathulla Khan, Department of Mathematics, Sir Vishveshwaraiah Institute of Science and Technology, Madanapalle- 517325, India

1 Introduction

The dynamics of non-Newtonian fluids has been a popular area of research owing to ever-increasing applications in chemical and process engineering. Examples of such fluids include coal-oil slurries, shampoo, paints, clay coating and suspensions, grease, cosmetic products, custard, physiological liquids (blood, bile, synovial fluid), fabricarion, pharmacology, polymer synthesis and food processing. In these applications, the working fluid is generically rheological in nature and the constitutive relationship between stress and rate of strain is non-linear in comparison to the Navier-Stokes equations. The rheology of these fluids manifests in many complex characteristic including fading memory, relaxation, elongational stresses, spin of suspended particles, retardation and adhesion. In general, the mathematical problems in non-Newtonian fluids are more complicated in comparison to the viscous Newtonian fluids. Despite their complexities, researchers are engaged in non-Newtonian fluid dynamics since the analysis and implementation of these fluids is critical to many diverse systems in biotechnology, chemical gels, manufacture of plastics, medical engineering, etc. The viscoelastic features in non-Newtonian fluids add more complexities in the resulting equations when compared with Navier–Stokes equations. Significant attention has been directed at the mathematical and numerical simulation of non-Newtonian fluids. Recent investigations on non-Newtonian fluids include, the Casson model [1], second-order Reiner-Rivlin differential fluid models [2], power-law nanoscale models [3], Eringen micro-morphic models [4], Eyring-Powell model [5], Tangent Hyperbolic fluid model [6], non-Newtonian Nanofluid model [7] and Jefferys viscoelastic model [8].

Convective heat transfer has mobilized substantial interest owing to its importance in industrial and environmental technologies including energy storage, gas turbines, nuclear plants, rocket propulsion, geothermal reservoirs, photovoltaic panels, etc. The convective boundary condition is simulated via a Biot number in the wall thermal boundary condition. Ishak [9] discussed the similarity solutions for flow and heat transfer over a permeable surface with convective boundary condition. Aziz [10] pro-

vided a similarity solution for laminar thermal boundary layer over a flat surface with a convective surface boundary condition. Makinde *et al.* [11] studied cross diffusion effects and Biot number influence on hydromagnetic Newtonian boundary layer flow with homogenous chemical reactions and MAPLE quadrature routines. Bég *et al.* [12] analyzed Biot number and buoyancy effects on magnetohydrodynamic thermal slip flows. Further studies include Abdul gaffar *et al.* [13–15].

Thermal radiation effects arise in nuclear engineering applications including reactors, propulsion systems, etc. When coupled with thermal convection flows, these transport phenomena problems are highly nonlinear. At a high temperature, the presence of thermal radiation changes the distribution of temperature in the boundary layer, which in turn affects the heat transfer at the wall. A variety of radiative heat transfer models have been utilized by thermal engineers. Rudraiah and Sasikumar [16] used the Milne-Eddington approximation and a Galerkin algorithm to simulate the stability of flow with conduction, convection and radiation heat transfer in a gray fluid-saturated sparsely packed non-Darcy porous medium. They observed the nature of the bounding surfaces and thermal radiation flux have a strong influence on the critical Rayleigh and wave numbers. Talukdar *et al.* [17] employed the Chandrasekhar discrete transfer method (DTM) to simulate radiative-convective flow in a porous medium channel. Yih [18] used the Rosseland diffusion flux approximation to analyze computationally mixed convective-radiative flow from a wedge geometry embedded in a non-Darcian porous medium. Takhar *et al.* [19] used the Cogley-Vincenti-Giles differential flux model to study radiative-convective boundary layer flow in a Darcy-Forchheimer porous regime with a numerical code. Chamkha *et al.* [20] studied radiation effects on mixed convection about a cone embedded in a fluid saturated porous medium filled with a nano fluid.

The boundary layer flows of non-Newtonian fluids have been widely recognized by the researchers in view of their immense technological and scientific applications such as polymer and food processing, oil recovery, etc. Most non-Newtonian models involve some form of modification to the momentum conservation equation (Newton's second law). Among the several non-Newtonian fluid models emerged, the differential type fluid models are very popular. The second-grade viscoelastic fluid model is the simplest model that describes the normal stress differences but cannot predict the shear thinning/thickening characteristics. However, the third-grade fluid model is capable of predicting both normal stresses and shear thinning/thickening characteristics. Many researchers have

examined the flows of third-grade fluid for various scenarios, usually with a mathematical emphasis and very little if any, physical understanding or interpretation of the solutions. Therefore, these studies are of very limited value to engineers who primarily work on complex (polymeric) fluid mechanics industries. For instance, the two-dimensional boundary layer flow of a third order fluid over a stretching sheet has been studied by Sajid and Hayat [21]. The analytic solution of the differential system was developed by homotopy analysis method (HAM). Sajid *et al.* [22] extended the analysis of ref. [21] by incorporating the MHD and heat transfer effects. Unsteady flow with heat and mass transfer of a third grade fluid has been discussed by Hayat *et al.* [23]. Sahoo [24] numerically investigated the Heimez flow and heat transfer of a third grade fluid. Slip effects on the third grade fluid flow driven by the stretching surface have been addressed by Sahoo and Do [25]. The above studies did not even attempt to evaluate the physical effects of third grade fluid making them of minimal interest from an engineering perspective. Abdul gaffar *et al.* [26] examined the radiative MHD flows of third-grade viscoelastic fluid past an isothermal inverted cone.

In many chemical engineering and nuclear process systems, *curvature of the vessels employed* is a critical aspect of optimizing thermal performance. Examples of curved bodies featuring in process systems include torus geometries, wavy surfaces, cylinders, cones, ellipses, oblate spheroids and spherical geometries. A number of theoretical and computational studies have been communicated on transport phenomena from cylindrical bodies, which frequently arise in polymer processing systems. These Newtonian studies were focused more on heat transfer aspects and include Eswara and Nath [27], Rotte and Beek [28] and the pioneering analysis of Sakiadis [29]. Further, studies examining multi-physical and chemical transport from cylindrical bodies include Zueco *et al.* [30]. An early investigation of rheological boundary layer heat transfer from a horizontal cylinder was presented by Chen and Leonard [31] who considered the power-law model and demonstrated that the transverse curvature has a strong effect on skin friction at moderate and large distances from the leading edge of the boundary layer. Lin and Chen [32] also studied axisymmetric laminar boundary-layer convection flow of a power-law non-Newtonian fluid over both a circular cylinder and a spherical body using the Merk-Chao series solution method. Pop *et al.* [33] simulated numerically the steady laminar forced convection boundary layer of power-law non-Newtonian fluid on a continuously moving cylinder with the surface maintained at a uniform temperature or uniform heat flux. Further, non-Newtonian models employed in analyzing convection

flows from cylinders include micropolar liquids [34], viscoelastic materials [35], micropolar nanofluids [36], unsteady convection in Nanofluid [37] and Casson fluids [1].

The objective of the present study is to investigate the steady, laminar convection boundary layer flow and heat transfer of a third grade viscoelastic fluid from a horizontal circular cylinder with thermal radiation and biot number effects. The non-dimensional equations with associated dimensionless boundary conditions constitute a highly nonlinear, coupled two-point boundary value problem. Keller’s implicit finite difference box scheme is implemented to solve the problem [26]. The effects of the emerging thermophysical parameters, namely the *third grade fluid parameter* (ϕ), the *material fluid parameters* (ϵ_1, ϵ_2), *thermal radiation* (F), *Biot number* (y) and *Prandtl number* (Pr) on velocity, temperature, skin friction number and heat transfer rate (local Nusselt number) characteristics are studied. Validation with earlier Newtonian solutions is also documented. The present problem has to the authors’ knowledge not appeared thus far in the scientific literature and is relevant to polymeric manufacturing processes in chemical engineering.

2 Constitutive equations for third-grade fluid

In the present study a subclass of viscoelastic fluids known as the *third grade fluid* is employed owing to its simplicity. This model physically captures the viscoelastic characteristics of certain polymers [38, 39]. The Cauchy stress tensor, of the *third grade* non-Newtonian fluid following Truesdell and Noll [40] takes the form:

$$\tau = -pI + \mu A_1 + \alpha_1 A_2 + \alpha_2 A_1^2 + \beta_1 A_3 + \beta_2 (A_1 A_2 + A_2 A_1) + \beta_3 (tr A_1^2) A_1 \tag{1}$$

where τ is the extra stress tensor, p is the pressure, I is the identity tensor, α_i ($i = 1, 2$), β_j ($j = 1, 2, 3$) are material constants and A_k ($k = 1, 2, 3$) are the first Rivlin-Ericksen tensors [35] which are defined by the following equations:

$$A_1 = (\nabla V) + (\nabla V)^T \tag{2}$$

$$A_n = \frac{dA_{n-1}}{dt} + A_{n-1} (\nabla V) + A_{n-1} (\nabla V)^T; \quad n > 1 \tag{3}$$

Here $\frac{d}{dt}$ is the material time derivative, (V) is the velocity and ∇ is an operator. We note that for $\beta_i = 0$, ($i = 1, 2, 3$), the model corresponds to the case of a second grade fluid.

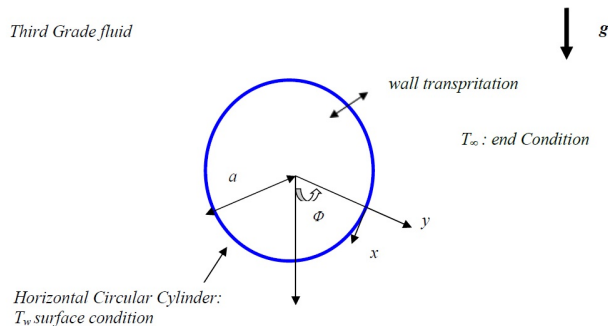


Fig. 1: Physical model and coordinate system

In order to satisfy the Clausius–Duhem inequality and the assumption that the Helmholtz free energy is minimum in equilibrium provide the following restrictions [41, 42].

$$\mu \geq 0, \quad \alpha_1 \geq 0, \quad \alpha_1 + \alpha_2 = 0 \tag{4}$$

And for third grade fluid [42],

$$\mu \geq 0, \quad \alpha_1 \geq 0, \quad |\alpha_1 + \alpha_2| \leq \sqrt{24\mu\beta_3}, \tag{5}$$

$$\beta_1 = 0, \quad \beta_2 = 0, \quad \beta_3 \geq 0$$

A comprehensive discussion on the restrictions for the material constants is made in detail by Dunn and Rajagopal [42]. The introduction of the appropriate terms into the flow model is considered next. The resulting boundary value problem is found to be well-posed and permits an excellent mechanism for the assessment of rheological characteristics on the flow behaviour.

3 Mathematical flow model

A steady, double-diffusive, laminar, incompressible flow and thermal convection of third-grade viscoelastic fluid from a horizontal cylinder with thermal radiation and Biot number effect, is considered, as illustrated in Fig. 1. The x -coordinate (tangential) is measured along the circumference of the cylinder from the lowest point and the y -coordinate (radial) is directed perpendicular to the surface, with a denoting the radius of the cylinder. $\Phi = x/a$ is the angle of the y -axis with respect to the vertical $0 \leq \Phi \leq \pi$. The gravitational acceleration g , acts downwards. We also assume that the Boussineq approximation holds *i.e.* the density variation is only experienced in the buoyancy term in the momentum equation. Both cylinder and third-grade fluid are maintained at the same constant temperature. Instantaneously, it is raised to a temperature $T_w > T_\infty$, the ambient temperature of the fluid which remains

unchanged. In line with Sahoo [24] and Hayat [23] and introducing the boundary layer approximations, the equations for *continuity, momentum and energy*, can be written as follows:

$$\frac{\partial u}{\partial x} + \frac{\partial v}{\partial y} = 0 \tag{6}$$

$$u \frac{\partial u}{\partial x} + v \frac{\partial u}{\partial y} = \nu \frac{\partial^2 u}{\partial y^2} + \frac{\alpha_1}{\rho} \left[u \frac{\partial^3 u}{\partial x \partial y^2} + v \frac{\partial^3 u}{\partial y^3} + \frac{\partial u}{\partial x} \frac{\partial^2 u}{\partial y^2} \right] + \frac{1}{\rho} [3\alpha_1 + 2\alpha_2] \frac{\partial u}{\partial y} \frac{\partial^2 u}{\partial x \partial y} + \frac{6\beta_3}{\rho} \left(\frac{\partial u}{\partial y} \right)^2 \frac{\partial^2 u}{\partial y^2} + g\beta(T - T_\infty) \sin(x/a) \tag{7}$$

$$u \frac{\partial T}{\partial x} + v \frac{\partial T}{\partial y} = \alpha \frac{\partial^2 T}{\partial y^2} - \frac{1}{\rho c_p} \frac{\partial q_r}{\partial y} \tag{8}$$

Where u and v are velocity components in x - and y - direction respectively, $\nu = \mu/\rho$ is the kinematic viscosity, β is the coefficient of thermal expansion, α is the thermal diffusivity, T is the temperature, ρ is the density of the fluid, c_p is the specific heat at constant pressure, q_r is the radiative heat flux and $\alpha_1, \alpha_2, \beta_3$ are the material constants. The third-grade fluid model introduces a number of *mixed* derivative into the momentum boundary layer equation (7). The momentum equation therefore attains an order higher than the *classical Navier-Stokes (Newtonian) viscous flow* model. The non-Newtonian effects feature in the shear terms only of eqn. (7) and not the convective (acceleration) terms. The fifth term on the right hand side of eqn. (7) represents the *thermal buoyancy force* and couples the velocity field with the temperature field equation. The appropriate boundary conditions are:

$$\begin{aligned} \text{At } y = 0, \quad & u = v = 0, \quad -k \frac{\partial T}{\partial y} = h_w (T_w - T) \\ \text{As } y \rightarrow \infty, \quad & u \rightarrow 0, \quad v \rightarrow 0, \quad T \rightarrow T_\infty \end{aligned} \tag{9}$$

Here T_∞ is the free stream temperature, k is the thermal conductivity, h_w is the convective heat transfer coefficient and T_w is the convective fluid temperature. In eqn. (8) the penultimate term on the right hand side is the *thermal radiation flux contribution* based on the Rosseland approximation [43]. This formulation allows the transformation of the governing integro-differential equation for radiative energy balance into a *Fourier-type* diffusion equation analogous to that describing heat conduction or electrostatic potential (Coulomb's law) which is valid for *optically-thick media* in which radiation only propagates a limited distance prior to experiencing scattering or absorption. It can be shown that the local intensity is caused by radiation emanating from nearby locations in the vicinity of which the emission and scattering are comparable to the location under consideration. For zones where conditions are

appreciably different, the radiation has been shown to be greatly attenuated prior to arriving at the location being analyzed. The energy transfer depends only on the conditions in the area near the position under consideration. In applying the Rosseland assumption, it is assumed that refractive index of the medium is constant, intensity within the porous medium is nearly isotropic and uniform and wavelength regions exist where the optical thickness is greater than 5. The Rosseland diffusion flux model is an *algebraic approximation* and defined as follows:

$$q_r = -\frac{4\sigma^* \partial T^4}{3k^* \partial y} \tag{10}$$

Where k^* is the mean absorption coefficient and σ^* is the Stefan-Boltzmann constant. It is customary [44] to express T^4 as a linear function of temperature. Expanding T^4 using Taylor series and neglecting higher order terms leads to:

$$T^4 \cong 4T_\infty^3 T - 3T_\infty^4 \tag{11}$$

Substituting (11) into (10), eventually leads to the following version of the heat conservation equation (8):

$$u \frac{\partial T}{\partial x} + v \frac{\partial T}{\partial y} = \alpha \frac{\partial^2 T}{\partial y^2} + \frac{16\sigma^* T_\infty^3}{3k^* \rho c_p} \frac{\partial^2 T}{\partial y^2} \tag{12}$$

The stream function ψ is defined by $u = \frac{\partial \psi}{\partial y}$ and $v = -\frac{\partial \psi}{\partial x}$, and therefore, the continuity equation is automatically satisfied. In order to render the governing equations and boundary conditions in dimensionless form, the following non-dimensional quantities are introduced.

$$\xi = \frac{x}{a}, \quad \eta = \frac{y}{a} Gr^{\frac{1}{4}}, \quad \psi = \nu Gr^{\frac{1}{4}} \xi f, \quad \theta(\xi, \eta) = \frac{T - T_\infty}{T_w - T_\infty} \tag{13}$$

In view of the transformation defined in eqn. (13), the governing eqns. (7) and (12) reduce to the following coupled, nonlinear, dimensionless partial differential equations for momentum and energy for the regime:

$$\begin{aligned} f'''' + f f'' - (f')^2 + \varepsilon_1 [2f' f'''' - f f^{iv}] + (3\varepsilon_1 + 2\varepsilon_2) (f'')^2 \\ + 6\varphi \xi^2 (f'')^2 f'''' + \theta \frac{\sin \xi}{\xi} \\ = \xi \left[f' \frac{\partial f'}{\partial \xi} - f'' \frac{\partial f}{\partial \xi} - \varepsilon_1 \left(f' \frac{\partial f''''}{\partial \xi} + f'''' \frac{\partial f'}{\partial \xi} - f^{iv} \frac{\partial f}{\partial \xi} \right) \right. \\ \left. - (3\varepsilon_1 + 2\varepsilon_2) f'' \frac{\partial f''}{\partial \xi} \right] \end{aligned} \tag{14}$$

$$\frac{\theta''}{Pr} \left[1 + \frac{4F}{3} \right] + f \theta' = \xi \left(f' \frac{\partial \theta}{\partial \xi} - \theta' \frac{\partial f}{\partial \xi} \right) \tag{15}$$

The transformed dimensionless boundary conditions are:

$$\begin{aligned} \text{At } \eta = 0, \quad & f = 0 = f', \quad \theta = 1 + \frac{\theta'}{\gamma} \\ \text{As } \eta \rightarrow \infty, \quad & f' \rightarrow 0, \quad f'' \rightarrow 0, \quad \theta \rightarrow 0 \end{aligned} \tag{16}$$

Here primes denote the differentiation with respect to η and $y = \frac{ah_w}{kl} Gr^{-1/4}$ is the Biot number, $\varphi = \frac{\beta_3 v}{\rho a^4} Gr^{3/2}$ is the third-grade fluid parameter, $\varepsilon_1 = \frac{\alpha_1 Gr^{1/2}}{\rho a^2}$ and $\varepsilon_2 = \frac{\alpha_2 Gr^{1/2}}{\rho a^2}$ are the material fluid parameters, $Pr = \frac{\nu}{\alpha}$ is the Prandtl number, $Gr = \frac{g\beta(T_w - T_\infty)a^3}{\nu^2}$ is the Grashof number and $F = \frac{4\sigma^* T_\infty^3}{k k^*}$ is the radiation parameter. The wall thermal boundary condition in (16) corresponds to convective cooling. The dimensionless skin-friction coefficient (shear stress at the cylinder surface) and dimensionless Nusselt number (heat transfer rate) are defined using the transformations described above with the following expressions.

$$C_f Gr^{\frac{1}{4}} = \xi \left[f''(\xi, 0) + \varepsilon_1 (3f'(\xi, 0)f''(\xi, 0) - f(\xi, 0)f'''(\xi, 0)) + 2\varphi\xi^2 (f''(\xi, 0))^3 \right] \tag{17}$$

$$Gr^{-1/4} Nu = -\theta'(\xi, 0) \tag{18}$$

The location, $\xi \sim 0$, corresponds to the vicinity of the lower stagnation point on the cylinder.

Since $\frac{\sin \xi}{\xi} \rightarrow 0/0$ i.e. 1. For this scenario, the model defined by eqns. (14) and (15) contracts to an ordinary differential boundary value problem:

$$f'''' + ff'' - (f')^2 + \varepsilon_1 [2f'f'' - ff^{iv}] + (3\varepsilon_1 + 2\varepsilon_2) (f'')^2 + \theta = 0 \tag{19}$$

$$\frac{\theta''}{Pr} \left[1 + \frac{4F}{3} \right] + f\theta' = 0 \tag{20}$$

The general model is solved using a powerful and unconditionally stable finite difference technique introduced by Keller [45]. The Keller-box method has a second order accuracy with arbitrary spacing and attractive extrapolation features. This method converges quickly and is ideal for parabolic problems.

4 Numerical solution with Keller-Box implicit method

The Keller-Box implicit difference method is implemented to solve the nonlinear boundary value problem defined by eqns. (14) – (15) with boundary conditions (16). This technique, despite recent developments in other numerical methods, remains a powerful and very accurate approach for parabolic boundary layer flows. It is unconditionally stable and achieves exceptional accuracy [45]. Recently, this method has been deployed in resolving many challenging and multi-physical fluid dynamics problems. The Keller-Box discretization is *fully coupled* at each step

which reflects the physics of parabolic systems – which are also fully coupled. Discrete calculus associated with the Keller-Box scheme has also been shown to be fundamentally different from all other mimetic (physics capturing) numerical methods, as elaborated by Keller [45]. The Keller-Box Scheme comprises four stages:

- 1) Decomposition of the N^{th} order partial differential equation system to N first order equations.
- 2) Finite Difference Discretization.
- 3) Quasilinearization of Non-Linear Keller Algebraic Equations and finally.
- 4) Block-tridiagonal Elimination solution of the Linearized Keller Algebraic Equations

Stage 1: Decomposition of N^{th} order partial differential equation system to N first order equations

Equations (14) – (15) subject to the boundary conditions (16) are first cast as a multiple system of first order differential equations. New dependent variables are introduced:

$$\begin{aligned} u(x, y) &= f', & v(x, y) &= f'', & q(x, y) &= f''', \\ s(x, y) &= \theta, & t(x, y) &= \theta' \end{aligned} \tag{21}$$

These denote the variables for velocity and temperature respectively. Now Equations (14) – (15) are solved as a set of sixth order simultaneous differential equations:

$$f' = u \tag{22}$$

$$u' = v \tag{23}$$

$$v' = q \tag{24}$$

$$s' = t \tag{25}$$

$$\begin{aligned} v' + fv - u^2 + \varepsilon_1 [2uq - fq'] + (3\varepsilon_1 + 2\varepsilon_2)v^2 + 6\phi\xi^2 v^2 q \\ + s \frac{\sin \xi}{\xi} = \xi \left[u \frac{\partial u}{\partial \xi} - v \frac{\partial f}{\partial \xi} - \varepsilon_1 \left(u \frac{\partial q}{\partial \xi} + q \frac{\partial u}{\partial \xi} - q' \frac{\partial f}{\partial \xi} \right) \right. \\ \left. - (3\varepsilon_1 + 2\varepsilon_2) v \frac{\partial v}{\partial \xi} \right] \end{aligned} \tag{26}$$

$$\frac{t'}{Pr} \left[1 + \frac{4F}{3} \right] + ft = \xi \left(u \frac{\partial s}{\partial \xi} - t \frac{\partial f}{\partial \xi} \right) \tag{27}$$

In terms of the dependent variables, the boundary conditions assume the form:

$$\begin{aligned} \text{At } \eta = 0, & \quad f = 0, \quad u = 0, \quad s = 1 + \frac{t}{y} \\ \text{As } \eta \rightarrow \infty, & \quad u \rightarrow 0, \quad v \rightarrow 0, \quad s \rightarrow 0 \end{aligned} \tag{28}$$

Stage 2: Finite Difference Discretization

A two dimensional computational grid is imposed on the ξ - η plane as depicted in Fig. 2. The stepping process is defined by:

$$\eta_0 = 0, \quad \eta_i = \eta_{i-1} + h_j, \quad j = 1, 2, \dots, J, \quad \eta_J \equiv \eta_\infty \tag{29}$$

$$\xi^0 = 0, \quad \xi^n = \xi^{n-1} + k_n, \quad n = 1, 2, \dots, N \tag{30}$$

Where k_n is the $\Delta\xi$ - spacing and h_j is the $\Delta\eta$ - spacing. If g_j^n denotes the value of any variable at (η_j, ξ^n) , then the variables and derivatives of equations (22) – (27) at $(\eta_{j-1/2}, \xi^{n-1/2})$ are replaced by:

$$g_{j-1/2}^{n-1/2} = \frac{1}{4} (g_j^n + g_{j-1}^n + g_j^{n-1} + g_{j-1}^{n-1}) \tag{31}$$

$$\left(\frac{\partial g}{\partial \eta}\right)_{j-1/2}^{n-1/2} = \frac{1}{2h_j} (g_j^n - g_{j-1}^n + g_j^{n-1} - g_{j-1}^{n-1}) \tag{32}$$

$$\left(\frac{\partial g}{\partial \xi}\right)_{j-1/2}^{n-1/2} = \frac{1}{2k_n} (g_j^n - g_{j-1}^n + g_j^{n-1} - g_{j-1}^{n-1}) \tag{33}$$

The finite-difference approximation of eqns. (22) – (27) for the mid-point $(\eta_{j-1/2}, \xi^n)$, are:

$$h_j^{-1} (f_j^n - f_{j-1}^n) = u_{j-1/2}^n \tag{34}$$

$$h_j^{-1} (u_j^n - u_{j-1}^n) = v_{j-1/2}^n \tag{35}$$

$$h_j^{-1} (v_j^n - v_{j-1}^n) = q_{j-1/2}^n \tag{36}$$

$$h_j^{-1} (s_j^n - s_{j-1}^n) = t_{j-1/2}^n \tag{37}$$

$$\begin{aligned} & (v_j - v_{j-1}) + \frac{h_j(1 + \alpha)}{4} (f_j + f_{j-1}) (v_j + v_{j-1}) - (1 + \alpha) \frac{h_j}{4} (u_j + u_{j-1})^2 + \frac{\epsilon_1 h_j (1 + \alpha)}{2} (u_j + u_{j-1}) (q_j + q_{j-1}) \\ & - \frac{\epsilon_1 (1 + \alpha)}{2} (f_j + f_{j-1}) (q_j - q_{j-1}) + (3\epsilon_1 + 2\epsilon_2) \frac{h_j (1 + \alpha)}{4} (v_j + v_{j-1})^2 + 6\phi\xi^2 \frac{h_j}{8} (v_j + v_{j-1})^2 (q_j + q_{j-1}) + \frac{h_j}{2} B (s_j + s_{j-1}) \\ & - \frac{\alpha h_j}{2} f_{j-1/2}^{n-1} (v_j + v_{j-1}) + \frac{\alpha h_j}{2} v_{j-1/2}^{n-1} (f_j + f_{j-1}) + \alpha \epsilon_1 f_{j-1/2}^{n-1} (q_j - q_{j-1}) - \frac{\alpha \epsilon_1}{2} (q')_{j-1/2}^{n-1} (f_j + f_{j-1}) = [R_1]_{j-1/2}^{n-1} \end{aligned} \tag{38}$$

$$\begin{aligned} & \frac{1}{Pr} \left[1 + \frac{4F}{3} \right] (t_j - t_{j-1}) + \frac{(1 + \alpha) h_j}{4} (f_j + f_{j-1}) (t_j + t_{j-1}) - \frac{\alpha h_j}{4} (u_j + u_{j-1}) (s_j + s_{j-1}) + \frac{\alpha h_j}{2} s_{j-1/2}^{n-1} (u_j + u_{j-1}) \\ & - \frac{\alpha h_j}{2} u_{j-1/2}^{n-1} (s_j + s_{j-1}) - \frac{\alpha h_j}{2} f_{j-1/2}^{n-1} (t_j + t_{j-1}) + \frac{\alpha h_j}{2} t_{j-1/2}^{n-1} (f_j + f_{j-1}) = [R_3]_{j-1/2}^{n-1} \end{aligned} \tag{39}$$

Where we have used the abbreviations:

$$\alpha = \frac{\xi^{n-1/2}}{k_n}, \quad B = \frac{\sin \xi^{n-1/2}}{\xi^{n-1/2}} \tag{40}$$

$$[R_1]_{j-1/2}^{n-1} = -h_j \left[\begin{aligned} & (v')_{j-1/2}^{n-1} + (1 - \alpha) (f v)_{j-1/2}^{n-1} - (1 - \alpha) (u_{j-1}^{n-1})^2 + 2\epsilon_1 (1 - \alpha) (u q)_{j-1/2}^{n-1} \\ & - \epsilon_1 (1 - \alpha) (f q')_{j-1}^{n-1} + 6\phi\xi^2 (v^2 q)_{j-1}^{n-1} + (1 - \alpha) (3\epsilon_1 + 2\epsilon_2) (v_{j-1}^{n-1})^2 + B s_{j-1/2}^{n-1} \end{aligned} \right] \tag{41}$$

$$[R_2]_{j-1/2}^{n-1} = -h_j \left[\frac{1}{Pr} \left[1 + \frac{4F}{3} \right] (t')_{j-1/2}^{n-1} + (1 - \alpha) (ft)_{j-1/2}^{n-1} + \alpha (us)_{j-1/2}^{n-1} \right] \tag{42}$$

The boundary conditions are:

$$f_0^n = u_0^n = 0, \quad s_0^n = 1, \quad u_j^n = 0, \quad v_j^n = 0, \quad s_j^n = 0 \tag{43}$$

Stage 3: Quasilinearization of Non-Linear Keller Algebraic Equations

Assuming $f_j^{n-1}, u_j^{n-1}, v_j^{n-1}, q_j^{n-1}, s_j^{n-1}, t_j^{n-1}$ to be known for $0 \leq j \leq J$, this leads to a system of $6J + 6$ equations for the solution of $6J + 6$ unknowns $f_j^n, u_j^n, v_j^n, q_j^n, s_j^n, t_j^n$, $j = 0, 1, 2, \dots, J$. This non-linear system of algebraic equations is linearized by means of Newton’s method.

Stage 4: Block-tridiagonal Elimination Solution of Linear Keller Algebraic Equations

The linearized system is solved by the block-elimination method, since it possesses a block-tridiagonal structure. The block-tridiagonal structure generated consists of block matrices. The complete linearized system is formulated as a block matrix system, where each element in the coefficient matrix is a matrix itself and this system is solved using the efficient Keller-box method. The numerical results are strongly influenced by the number of mesh points in both directions. After some trials in η -direction (radial coordinate), a larger number of mesh points are selected whereas in ξ -direction (tangential coordinate) significantly less mesh points are utilized. η_{max} has been set at 16 and this defines an adequately large value at which the prescribed boundary conditions are satisfied. ξ_{max} is set at 3.0 for this flow domain. Mesh independence is achieved in the present computations. The numerical algorithm is executed in MATLAB on a PC. The method demonstrates excellent stability, convergence and consistency, as elaborated by Keller [45].

5 Numerical results and interpretation

Comprehensive solutions have been obtained and are presented in Tables 1 – 2 and Figs. 3– 13. The numerical problem comprises two independent variables (ξ, η), two dependent fluid dynamic variables (f, θ) and seven thermo-physical and body force control parameters, namely, $\phi, \epsilon_1, \epsilon_2, \gamma, F, Pr, \xi$. The following default parameter values i.e. $\phi = 0.1, \epsilon_1 = \epsilon_2 = 0.3, \gamma = 0.2, F = 0.5, Pr = 7.0$ and $\xi = 1.0$ are prescribed (unless otherwise stated). Furthermore, the influence of stream-wise (transverse) coordinate on heat transfer characteristics is also investigated. The comparison solutions are presented in Table 1 and shows an excellent correlation for the heat transfer rate for various values of ξ . Table 2 presents the influence of the third-grade fluid

parameter (ϕ) and the material fluid parameter (ϵ_1, ϵ_2) on dimensionless skin friction (C_f) and heat transfer rate ($-\theta'(\xi, 0)$). An increasing ϕ is observed to decrease both C_f and $-\theta'(\xi, 0)$. Furthermore, an increase in ϵ_1 enhances the skin friction but reduces heat transfer rate. However, an increase in ϵ_2 is seen to increase both skin friction and heat transfer rate. Table 3 document results for the influence of Biot number (γ) and Prandtl number (Pr) on dimensionless skin friction and heat transfer rate along with a variation in the radiation parameter (F). Both skin friction and heat transfer rate are observed to increase with increasing γ values. Whereas, increasing F is seen to reduce skin friction and enhance the heat transfer rate. Table 2 also presents the variations of skin friction and heat transfer rate for various values of Pr . It is observed that with increasing Pr , the skin friction is depressed but the heat transfer rate is elevated. By def., Pr is the relative rate of momentum diffusion to thermal diffusion. For $Pr > 1$, the momentum diffuses faster than the heat and vice versa for $Pr < 1$. For higher values of Pr , the thermal conductivity of the viscoelastic fluid is lowered. Therefore, increasing Pr lead to heating of the viscoelastic fluid and drops the heat transfer rate at the cylinder surface.

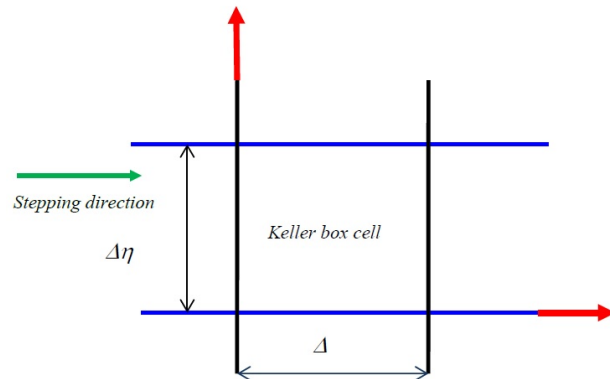


Fig. 2: Keller box computational cell

Fig. 3(a)–3(b) depicts the velocity (f') and temperature(θ) distributions with increasing third grade fluid parameter (ϕ). Very little tangible effect is observed in fig. 3a, although there is a slight decrease in velocity with increase in ϕ . From physical point of view, large values of ϕ weaken the shear thinning effect which leads to an increase in fluid viscosity and therefore causes a decreased in fluid velocity and the boundary layer thickness. Conversely, there is only a very slight increase in temperature magnitudes in Fig. 3(b) with a rise in ϕ . The mathematical model reduces to the Newtonian

Table 1: Values of the local heat transfer coefficient ($-\theta'(\xi, 0)$) for various values of ξ with $\phi = 0.0, \epsilon_1 = 0.0, \epsilon_2 = 0.0, y = 0.0, Pr = 7.0, F \rightarrow 0$

| ξ | $-\theta'(\xi, 0)$ | | |
|-------|--------------------|--------------------------|-----------------|
| | Merkin [48] | Nazar <i>et al.</i> [49] | Present results |
| 0.0 | 0.4212 | 0.4214 | 0.4213 |
| 0.4 | 0.4182 | 0.4184 | 0.4183 |
| 0.8 | 0.4093 | 0.4096 | 0.4095 |
| 1.2 | 0.3942 | 0.3950 | 0.3948 |
| 1.6 | 0.3727 | 0.3740 | 0.3738 |
| 2.0 | 0.3443 | 0.3457 | 0.3455 |
| 2.4 | 0.3073 | 0.3086 | 0.3083 |
| 2.8 | 0.2581 | 0.2595 | 0.2593 |
| π | 0.1963 | 0.1962 | 0.1961 |

Table 2: Values of C_f and $-\theta'(\xi, 0)$ for different φ, ϵ_1 and ϵ_2 ($Pr = 7.0, F = 0.5, y = 0.2, \xi = 1.0$)

| ϵ_1 | ϵ_2 | $\varphi = 0.0$ | | $\varphi = 5.0$ | | $\varphi = 10.0$ | | $\varphi = 20.0$ | | $\varphi = 30.0$ | |
|--------------|--------------|-----------------|--------------------|-----------------|--------------------|------------------|--------------------|------------------|--------------------|------------------|--------------------|
| | | C_f | $-\theta'(\xi, 0)$ | C_f | $-\theta'(\xi, 0)$ | C_f | $-\theta'(\xi, 0)$ | C_f | $-\theta'(\xi, 0)$ | C_f | $-\theta'(\xi, 0)$ |
| 0.1 | 0.3 | 0.2550 | 0.2210 | 0.2635 | 0.2085 | 0.2701 | 0.2025 | 0.2807 | 0.1952 | 0.2927 | 0.1906 |
| 0.6 | | 0.2604 | 0.2185 | 0.2671 | 0.2070 | 0.2730 | 0.2013 | 0.2833 | 0.1944 | 0.2962 | 0.1899 |
| 1.2 | | 0.2664 | 0.2157 | 0.2711 | 0.2054 | 0.2763 | 0.2000 | 0.2864 | 0.1934 | 0.3004 | 0.1891 |
| 1.5 | | 0.2692 | 0.2144 | 0.2730 | 0.2045 | 0.2779 | 0.1994 | 0.2879 | 0.1929 | 0.3025 | 0.1887 |
| 2.0 | | 0.2734 | 0.2123 | 0.2760 | 0.2032 | 0.2805 | 0.1983 | 0.2904 | 0.1921 | 0.3059 | 0.1880 |
| 0.3 | 0 | 0.2496 | 0.2189 | 0.2598 | 0.2073 | 0.2668 | 0.2016 | 0.2775 | 0.1946 | 0.2880 | 0.1868 |
| | 1 | 0.2766 | 0.2227 | 0.2775 | 0.2093 | 0.2820 | 0.2030 | 0.2936 | 0.1956 | 0.3142 | 0.1901 |
| | 2 | 0.3087 | 0.2268 | 0.2957 | 0.2112 | 0.2987 | 0.2044 | 0.3219 | 0.1966 | 0.3766 | 0.1908 |
| | 3 | 0.3479 | 0.2315 | 0.3157 | 0.2132 | 0.3213 | 0.2058 | 0.3924 | 0.1975 | 0.5508 | 0.1916 |
| | 4 | 0.3975 | 0.2369 | 0.3388 | 0.2151 | 0.3704 | 0.2073 | 0.6108 | 0.1975 | 1.6622 | 0.1919 |

Table 3: Values of C_f and $-\theta'(\xi, 0)$ for different y, Pr and F ($\varphi = 0.1, \epsilon_1 = 0.3 = \epsilon_2, \xi = 1.0$)

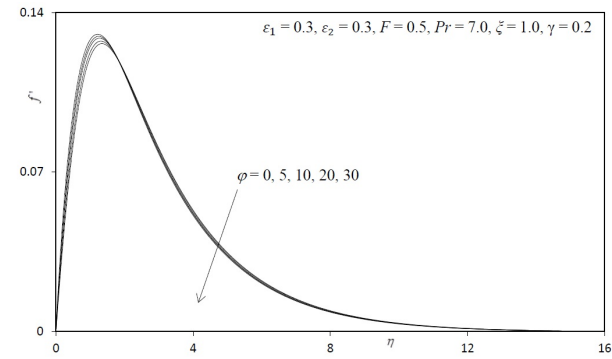
| y | Pr | $F = 0.0$ | | $F = 0.05$ | | $F = 0.1$ | | $F = 0.15$ | | $F = 0.2$ | |
|-----|--------|-----------|--------------------|------------|--------------------|-----------|--------------------|------------|--------------------|-----------|--------------------|
| | | C_f | $-\theta'(\xi, 0)$ | C_f | $-\theta'(\xi, 0)$ | C_f | $-\theta'(\xi, 0)$ | C_f | $-\theta'(\xi, 0)$ | C_f | $-\theta'(\xi, 0)$ |
| 0.2 | 7.0 | 0.2020 | 0.3012 | 0.2105 | 0.2862 | 0.2179 | 0.2740 | 0.2244 | 0.2638 | 0.2303 | 0.2550 |
| 0.3 | | 0.2833 | 0.5225 | 0.2954 | 0.4964 | 0.3059 | 0.4751 | 0.3153 | 0.4574 | 0.3237 | 0.4421 |
| 0.4 | | 0.3215 | 0.6410 | 0.3352 | 0.6090 | 0.3472 | 0.5829 | 0.3579 | 0.5611 | 0.3675 | 0.5423 |
| 0.5 | | 0.3437 | 0.7143 | 0.3585 | 0.6786 | 0.3714 | 0.6495 | 0.3828 | 0.6251 | 0.3932 | 0.6043 |
| 0.6 | | 0.3583 | 0.7640 | 0.3737 | 0.7257 | 0.3872 | 0.6946 | 0.3992 | 0.6686 | 0.4100 | 0.6462 |
| 0.2 | | 3 | 0.2438 | 0.2365 | 0.2536 | 0.2241 | 0.2620 | 0.2141 | 0.2695 | 0.2056 | 0.2763 |
| | 5 | 0.2179 | 0.2740 | 0.2269 | 0.2601 | 0.2347 | 0.2488 | 0.2416 | 0.2393 | 0.2479 | 0.2312 |
| | 7 | 0.2020 | 0.3012 | 0.2105 | 0.2862 | 0.2179 | 0.2740 | 0.2244 | 0.2638 | 0.2303 | 0.2550 |
| | 8 | 0.1960 | 0.3126 | 0.2042 | 0.2971 | 0.2114 | 0.2845 | 0.2179 | 0.2740 | 0.2236 | 0.2649 |
| 10 | 0.1862 | 0.3325 | 0.1941 | 0.3162 | 0.2011 | 0.3029 | 0.2072 | 0.2918 | 0.2128 | 0.2823 | |

viscous flow model as $\phi \rightarrow 0, \epsilon_1 \rightarrow 0$ and $\epsilon_2 \rightarrow 0$. The momentum boundary layer equation in this case contracts to the familiar equation for Newtonian convection from a cylinder, viz.

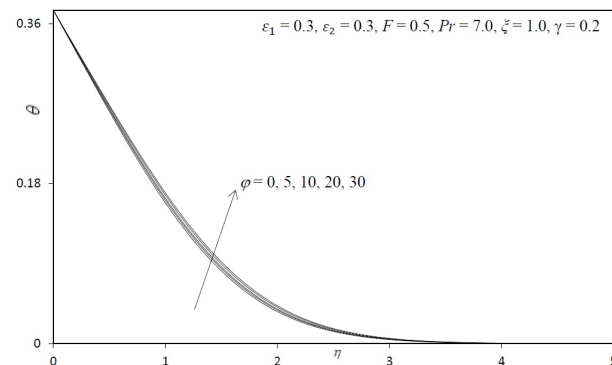
$$f''' + ff'' - (f')^2 + \theta \frac{\sin \xi}{\xi} = \xi \left[f' \frac{\partial f'}{\partial \xi} - f'' \frac{\partial f}{\partial \xi} \right].$$

The thermal boundary layer equation (15) remains unchanged. It is observed that if $\phi = 0$ and $\epsilon_1 = -\epsilon_2$, the governing equation reduces to the second-grade fluid.

Fig. 4(a)–4(b) illustrate the effects of the material fluid parameter, ϵ_1 , on velocity (f') and temperature (θ) distributions throughout the boundary layer regime. Velocity is seen to decrease with increasing ϵ_1 . This is due to the relaxation effect in the fluid further away from the surface of the cylinder resulting in shear-thickening and higher viscosity in the fluid. Conversely, temperature is consistently increased with increasing values of ϵ_1 . The higher values of ϵ_1 accompany with higher normal stress differences which increases the temperature.



(a)

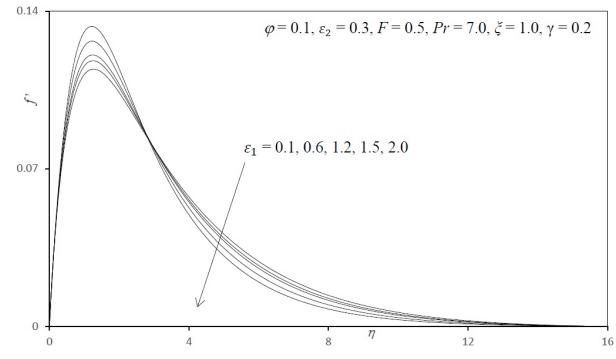


(b)

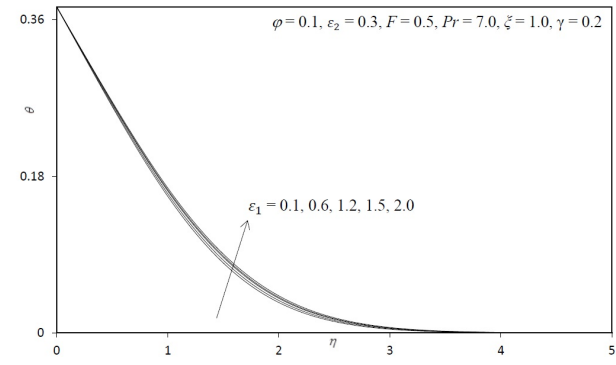
Fig. 3: (a) Effect of ϕ on Velocity Profiles; (b) Effect of ϕ on Temperature Profiles;

Fig. 5(a)–5(b) presents the effect of the *material fluid parameter*, ϵ_2 , on velocity (f') and temperature(θ) distributions throughout the boundary layer regime. Velocity is significantly increased with increasing ϵ_2 . It is evident that an increase in ϵ_2 corresponds to an increase in the normal stress differences which increase the fluid velocity. For greater values of ϵ_2 , the elasticity of the fluid increases whereas the viscosity reduces. Conversely, temperature is consistently reduced with increasing values of ϵ_2 . This results in a decrease in the heat diffusion rate.

Fig. 6(a)–6(b) depict the evolution of velocity (f') and temperature (θ) functions with a variation in Biot number, y . Dimensionless velocity component (Fig. 6a) is considerably enhanced with increasing y . In Fig. 6b, an increase in Biot number is seen to considerably enhance temperatures throughout the boundary layer regime. For $y < 1$ i.e. small Biot numbers, the regime is frequently designated as being “thermally simple” and there is a presence of more uniform temperature fields inside the boundary layer and the cylinder solid surface. For $y > 1$, thermal fields are anticipated to be non-uniform within the solid body. The Biot number effectively furnishes a mechanism for comparing the conduction resistance within a solid body to



(a)

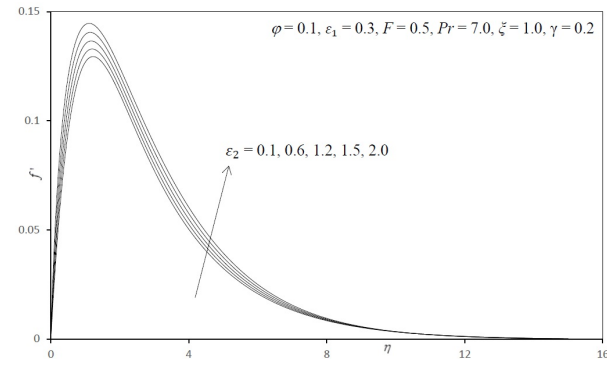


(b)

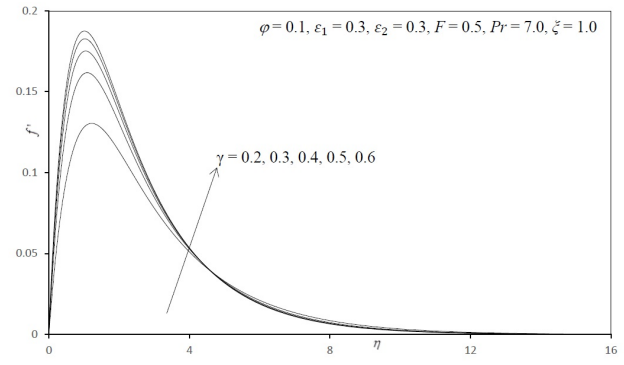
Fig. 4: (a) Effect of ϵ_1 on the Velocity Profiles; (b) Effect of ϵ_1 on Temperature Profiles

the convection resistance external to that body (offered by the surrounding fluid) for heat transfer. We also note that a Biot number in excess of 0.2, as studied in Figs. 6a, b corresponds to a “thermally thick” substance whereas Biot number less than 0.1 implies a “thermally thin” material. Since y is inversely proportional to thermal conductivity (k), as y increases, thermal conductivity will be reduced at the cylinder surface and this will lead to a decrease in the rate of heat transfer from the boundary layer to within the cylinder, manifesting in a rise in temperature at the cylinder surface and in the body of the fluid-the maximum effect will be sustained at the surface, as witnessed in Fig. 6b. However, for a fixed wall convection coefficient and thermal conductivity, Biot number as defined in $y = \frac{xh_w}{k} Gr^{-1/4}$ is inversely proportional to the local Grashof (free convection) number. As local Grashof number increases generally the enhancement in buoyancy causes a deceleration in boundary layer flows [46]; however as Biot number increases, the local Grashof number must decrease and this will induce the opposite effect i.e. accelerate the boundary layer flow, as shown in Fig. 6a.

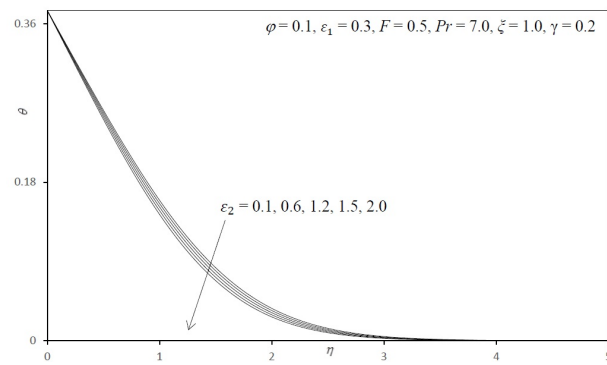
Fig. 7(a)–7(b) depicts the profiles for velocity (f') and temperature(θ)for various values of the radiation param-



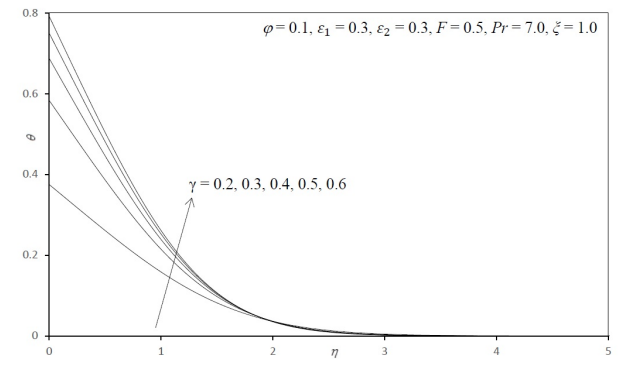
(a)



(a)



(b)



(b)

Fig. 5: (a) Effect of ϵ_2 on Velocity Profiles; b) Effect of ϵ_2 on Temperature Profiles

Fig. 6: (a) Effect of γ on Velocity Profiles; (b) Effect of γ on Temperature Profiles

ter, F . It is observed that an increase in F accelerates the flow i.e., velocity increases. Also, increasing F is found to enhance the temperature. Presence of radiation produces more heat to liquid. An increase in fluid temperature induces more flow in the boundary layer resulting in increasing of fluid velocity. An increasing radiation energizes the boundary layer and enhances the thermal energy and hence increases the thermal boundary layer thickness. For $F = 0$, the thermal conduction dominates i.e., the radiative flux vanishes and achieves minimum temperature. Hence it is confirmed that high temperature benefits the processing of materials with radiative transfer contribution. For $F < 1$, the thermal radiation contributes more than thermal conduction and vice versa for $F > 1$. For $F = 1$, both thermal radiation and conduction have the same contribution.

Fig. 8(a)–8(b) depict the velocity (f') and temperature (θ) distributions for various transverse (stream wise) coordinate values, ξ . Generally, velocity is noticeably lowered with increasing migration from the leading edge i.e. larger ξ values (Fig. 8a). The maximum velocity is computed at the lower stagnation point ($\xi \sim 0$) for low values of radial coordinate (η). The transverse coordinate clearly exerts a

significant influence on momentum development. A very strong increase in temperature (θ), as observed in Fig. 8b, is generated throughout the boundary layer with increasing ξ values. The temperature field decays monotonically. Temperature is maximized at the surface of the cylindrical body ($\eta = 0$, for all ξ) and minimized in the free stream ($\eta = 16$). Although the behaviour at the upper stagnation point ($\xi \sim \pi$) is not computed, the pattern in Fig. 8b suggests that temperature will continue to progressively grow here compared with previous locations on the cylinder surface (lower values of ξ).

Fig. 9(a)–9(b) present the influence of the third-grade fluid parameter, ϕ , on the dimensionless skin friction coefficient, C_f and heat transfer rate, $-\theta'(\xi, 0)$ at the cylinder surface. It is observed that C_f is decreased with an increase in ϕ values i.e. the boundary layer flow is accelerated with decreasing viscosity effects in the non-Newtonian regime. The surface heat transfer rate is substantially decreased with increasing ϕ values. This correlates well with the temperature computations discussed earlier. Since the temperature is reduced for greater values of ϕ , the heat transfer to the wall also falls i.e., heat transfer is enhanced to the body of fluid.

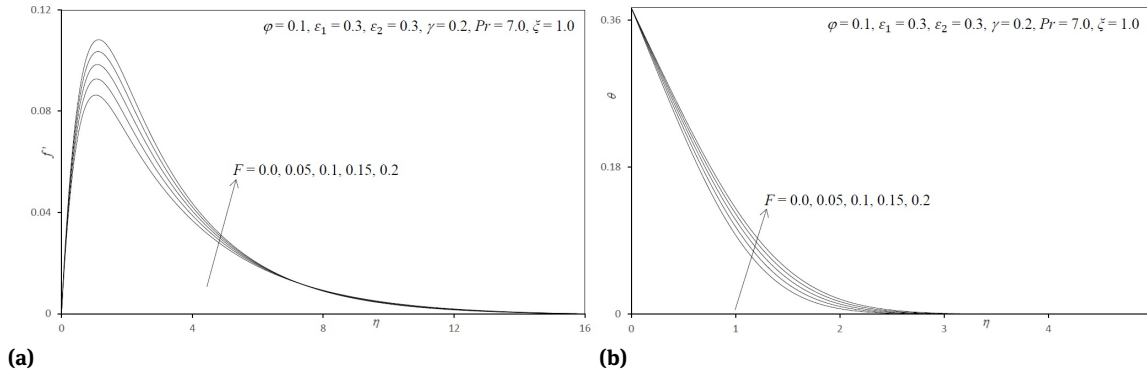


Fig. 7: (a) Effect of F on Velocity Profiles; (b) Effect of F on Temperature Profiles

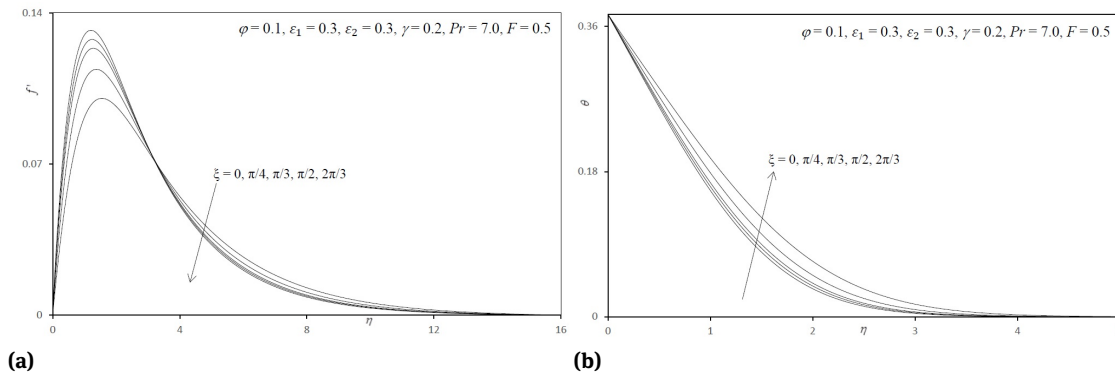


Fig. 8: (a) Effect of ζ on Velocity Profiles; (b) Effect of ζ on Temperature Profiles

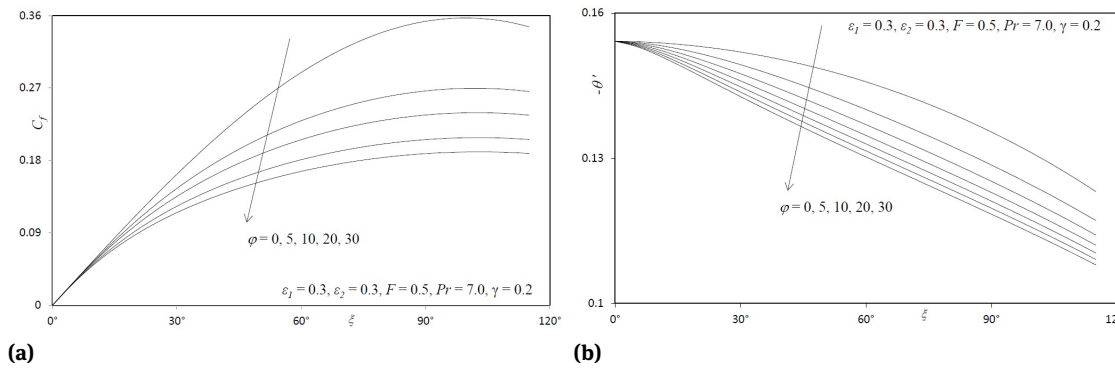


Fig. 9: (a) Effect of φ on Skin Friction; (b) Effect of φ on Nusselt number

Fig. 10(a)–10(b) illustrates the influence of the material fluid parameter, ϵ_1 , on the dimensionless skin friction coefficient, C_f and heat transfer rate, $-\theta'(\zeta, 0)$ at the cylinder surface. At the cylinder surface C_f is enhanced with increasing ϵ_1 , however only for very large values of the transverse coordinate, ζ . Whereas, heat transfer rate is reduced with increasing ϵ_1 , again at large values of ζ , as computed in Fig. 10b.

Fig. 11(a)–11(b) illustrates the influence of the material fluid parameter, ϵ_2 , on the dimensionless skin friction coefficient, C_f and heat transfer rate, $-\theta'(\zeta, 0)$ at the cylinder surface. The skin friction (fig. 11a) at the cylinder surface is enhanced with increasing ϵ_2 , however only for very large values of the transverse coordinate, ζ . The heat transfer rate is also enhanced with increasing ϵ_2 , again at large values of ζ , as computed in Fig. 11b.

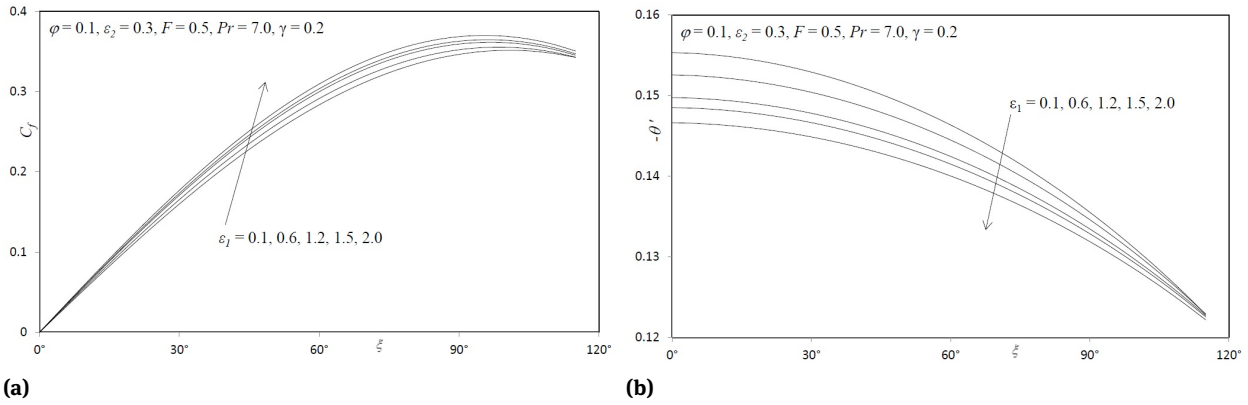


Fig. 10: (a) Effect of ϵ_1 on Skin Friction; (b) Effect of ϵ_1 on Nusselt number

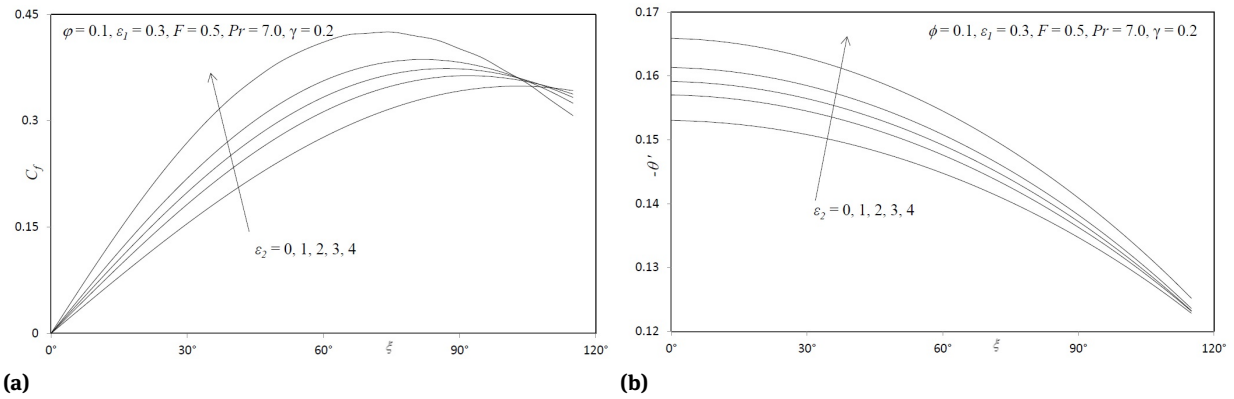


Fig. 11: (a) Effect of ϵ_2 on Skin Friction; (b) Effect of ϵ_2 on Nusselt number

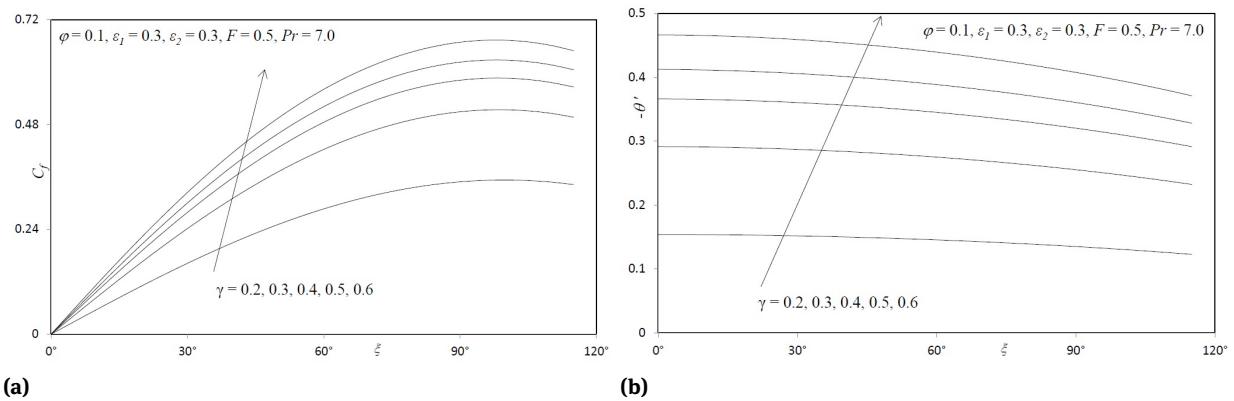


Fig. 12: (a) Effect of γ on Skin Friction; (b) Effect of γ on Nusselt number

Fig. 12(a)–12(b) presents the influence of the Biot number, γ , on the dimensionless skin friction coefficient, C_f and heat transfer rate, $-\theta'(\xi, 0)$ at the cylinder surface. The skin friction at the cylinder surface is found to greatly enhance with rising Biot number, γ . This is principally

attributable to the decrease in Grashof (free convection) number which results in an acceleration in the boundary layer flow, as elaborated by Chen and Chen [47]. Heat transfer rate is also enhanced with increasing γ , at large values of ξ , as computed in Fig. 12(b).

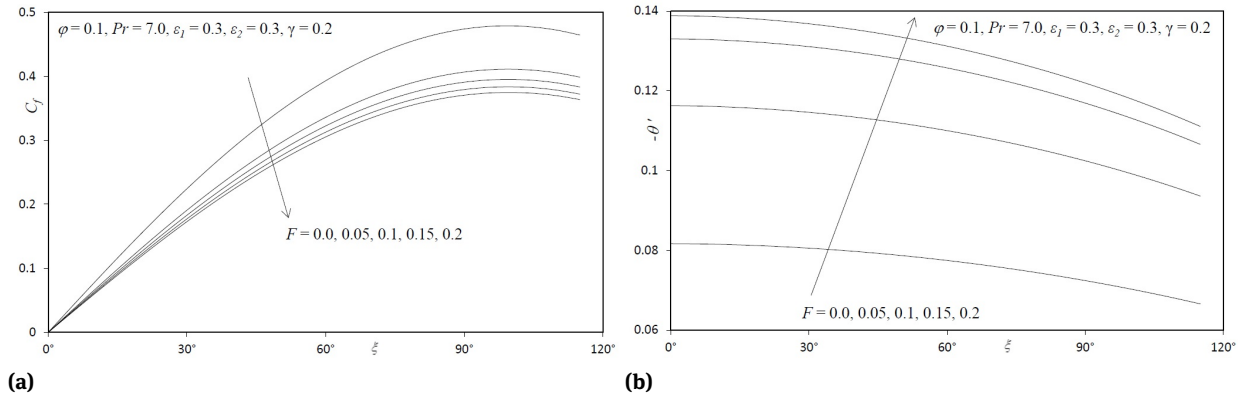


Fig. 13: (a) Effect of F on Skin Friction; (b) Effect of F on Nusselt number

Fig. 13(a)–13(b) depict the influence of the radiation parameter, F , on the dimensionless skin friction coefficient, C_f and heat transfer rate, $-\theta'(\xi, 0)$ at the cylinder surface. It is observed that C_f is decreased with an increase in F i.e., the thermal radiative flux magnitudes are decreased. The surface heat transfer rate is substantially *increased* with increasing F . The greater contribution of thermal conduction heat transfer and lower radiative contribution inhibits species diffusin to the cylinder surface.

6 Conclusions

Numerical solutions have been presented for the buoyancy-driven flow and heat transfer of third grade flow external to a horizontal circular cylinder. The Keller-box implicit second order accurate finite difference numerical scheme has been implemented to efficiently solve the transformed, dimensionless velocity and thermal boundary layer equations, subject to realistic boundary conditions. Excellent correlation with previous studies has been demonstrated testifying the validity of the present code. The computations have shown that:

1. Increasing third grade fluid parameter, ϕ , reduces the velocity, skin friction (surface shear stress) and heat transfer rate, whereas it elevates temperature in the boundary layer.
2. Increasing material fluid parameter, ϵ_1 , decreases the velocity and Nusselt number for all values of the radial coordinate whereas it increases temperature and skin friction.
3. Increasing material fluid parameter, ϵ_2 , increases the velocity, skin friction and Nusselt number whereas decreases temperature.

4. Increasing Biot number, γ , increases velocity, temperature, skin friction (surface shear stress) and heat transfer rate.

References

- [1] V. Ramachandra Prasad, A. Subba Rao, N. Bhaskar Reddy, B Vasu and O Anwar Bég, Modelling laminar transport phenomena in a Casson rheological fluid from a horizontal circular cylinder with partial slip, *Proc I MechE Part E: J Process Mechanical Engineering* Vol. 227, Issue 4, pp309-326, 2013. DOI: 10.1177/0954408912466350.
- [2] M. Norouzi, M. Davoodi, O. Anwar Bég and A.A. Joneidi, Analysis of the effect of normal stress differences on heat transfer in creeping viscoelastic Dean flow, *Int. J. Thermal Sciences* Vol. 69, pp.61-69, 2013.
- [3] M. J. Uddin, N. H. M. Yusoff, O. Anwar Bég and A. I. Ismail, Lie group analysis and numerical solutions for non-Newtonian nanofluid flow in a porous medium with internal heat generation, *Physica Scripta*, Vol. 87, No. 2, 025401, 2013.
- [4] M. M. Rashidi, M. Keimanesh, O. Anwar Bég, T. K. Hung, Magneto-hydrodynamic biorheological transport phenomena in a porous medium: A simulation of magnetic blood flow control, *Int. J. Numer. Meth. Biomed. Eng.*, Vol. 27, Issue 6, pp.805-821, 2011.
- [5] S. Abdul Gaffar, V. Ramachandra Prasad, O. Anwar Beg, Computational study of non-Newtonian Eyring-Powell fluid from a vertical porous plate with Biot number effects, *J. of the Brazilian Society of Mechanical Sciences and Engineering*, Vol. 39, Issue 7, pp.2747-2765, 2017.
- [6] S. Abdul Gaffar, V. Ramachandra Prasad, E. Keshava Reddy, Computational Study of MHD free convection flow of non-Newtonian Tangent Hyperbolic fluid from a vertical surface in porous media with Hall/Ionslip current and Ohmic dissipation, *Int. J. App. Comp. Math.*, Vol. 3, Issue 2, pp.859-890, 2017.
- [7] S. Abdul Gaffar, V. Ramachandra Prasad, O. Anwar Beg, Computational modelling and solutions for mixed convection boundary layer flows of Nanofluid from a non-isothermal wedge, *J. Nanofluid*, Vol. 7, No. 5, pp.1024-1032, 2018.

- [8] D. Tripathi, S.K. Pandey and O. Anwar Bég, Mathematical modelling of heat transfer effects on swallowing dynamics of viscoelastic food bolus through the human oesophagus, *Int. J. Thermal Sciences*, Vol. 70, pp. 41-53, 2013.
- [9] A. Ishak, Similarity solutions for flow and heat transfer over a permeable surface with convective boundary condition, *Appl. Math. Comput.* Vol. 217, Issue 2, pp.837–842, 2010.
- [10] A. Aziz, A similarity solution for laminar thermal boundary layer over a flat plate with a convective surface boundary condition, *Comm. Non. Sci. Num. Sim.*, Vol. 14, Issue 4, pp.1064–1068, 2009.
- [11] O. D. Makinde, K. Zimba, O. Anwar Bég, Numerical study of chemically-reacting hydromagnetic boundary layer flow with Soret/Dufour effects and a convective surface boundary condition, *Int. J. Thermal and Environmental Engineering*, Vol. 4, No. 1, pp.89-98, 2012.
- [12] O. Anwar Bég, M.J. Uddin, M.M. Rashidi and N. Kavyani, Double-diffusive radiative magnetic mixed convective slip flow with Biot number and Richardson number effects, *J. Engineering Thermophysics*, Vol. 23, Issue 2, pp.79-97, 2014.
- [13] S. Abdul Gaffar, V. Ramachandra Prasad, E. Keshava Reddy, Non-Newtonian thermal convection from an isothermal sphere with Biot number effects, *Int. J. of Industrial Mathematics*, Vol.8, No.2, 2016
- [14] S. Abdul Gaffar, V. Ramachandra Prasad, E. Keshava Reddy, O. Anwar Beg, Computational study of non-Newtonian thermal convection from a vertical porous plate in a non-Darcy porous medium with Biot number effects, *Journal of Porous Media*, Vol. 17, Issue 7, pp.601-622, 2014.
- [15] V. Ramachandra Prasad, S. Abdul gaffar, O. Anwar Beg, Mathematical study of laminar boundary layer flow and heat transfer of tangent hyperbolic fluid past a vertical porous plate with Biot number effects, *J. Applied Fluid Mechanics*. Vol. 9, No. 3, pp.1297-1307. 2016.
- [16] Rudraiah, N. and Sasikumar, T.P., Radiation and non-Darcy effects on convection in porous media, *Chemical Engineering Communications*, Vol. 87, Issue 1, pp.53-65, 1990.
- [17] Talukdar, P., Mishra, S.C., Trimis, D. and Durst, F., Combined radiation and convection heat transfer in a porous channel bounded by isothermal parallel plates, *Int. J. Heat Mass Transfer*, Vol. 47, Issue 5, pp.1001–1013, 2004.
- [18] Yih, K-A., Radiation effect on mixed convection over an isothermal wedge in porous media: the entire regime, *Heat Transfer Engineering*, Vol. 22, Issue 3, pp.26-32, 2001.
- [19] Takhar, H.S., Bég, O. Anwar and M. Kumari, Computational analysis of coupled radiation convection dissipative flow in a porous medium using the Keller-Box implicit difference scheme, *Int. J. Energy Research*, Vol. 22, Issue 2, pp.141-159, 1998.
- [20] A.J. Chamkha, S. Abbasbandy, A.M. Rashad and K. Vajravelu, Radiation Effects on Mixed Convection about a Cone Embedded in a Porous Medium Filled with a Nanofluid, *Meccanica* 48 (2013): 275-285.
- [21] Sajid, M., Hayat, T, Non-similar series solution for boundary layer flow of a third-order fluid over a stretching sheet, *Appl. Math. Comput.*, Vol. 189, Issue 2, pp.1576-1585, 2007.
- [22] Sajid, M., Hayat, T., Asghar, S., Non-similar analytic solution for MHD flow and heat transfer in a third order fluid over a stretching sheet, *Int. J. Heat Mass Transfer*, Vol. 50, Issue 9-10, pp.1723-1736, 2007.
- [23] Hayat, T., Mustafa, M., Asghar, S., Unsteady flow with heat and mass transfer of a third grade fluid over a stretching surface in the presence of chemical reaction, *Nonlinear Anal.: RWA*, Vol. 11, Issue 4, pp.3186-3197, 2010.
- [24] Sahoo, B., Heimenz flow and heat transfer of a third grade fluid, *Comm. Nonlinear Sci. Num. Simul.*, Vol. 14, Issue 3, pp.811-826, 2009.
- [25] Sahoo, B., Do, Y., Effects of slip on sheet driven flow and heat transfer of a third grade fluid pasta stretching sheet, *Int. Comm. Heat Mass Transfer*, Vol. 37, pp.1064-1071, 2010.
- [26] S. Abdul Gaffar, V. Ramachandra Prasad, O. Anwar Beg, Md. H. Hidayathullah Khan and K. Venkatadri, Radiative and Magneto-hydrodynamics flow of Third Grade viscoelastic fluid past an isothermal inverted cone in the presence of heat generation/absorption, *J. of the Brazilian Society of Mechanical Sciences and Engineering*, 2018. DOI:10.1007/s40430-018-1049-0. 2018.
- [27] Eswara, A.T. and Nath G., Unsteady forced convection laminar boundary layer flow over a moving longitudinal cylinder, *Acta Mech.*, Vol. 93, Issue 1-4, pp.13-28, 1992.
- [28] Rotte, J. W. and Beek, W.J., Some models for the calculation of heat transfer coefficients to moving continuous cylinders, *Chem. Eng. Sci.*, Vol. 24, Issue 4, pp.705-716, 1969.
- [29] Sakiadis, B.C., Boundary-layer behavior on continuous solid surfaces, III. The boundary layer on a continuous cylindrical surface, *AIChE. J.*, Vol. 7, Issue 3, pp.467-472, 1961.
- [30] Zueco, J., O. Anwar Bég, Tasveer A. Bég and H.S. Takhar, Numerical study of chemically-reactive buoyancy-driven heat and mass transfer across a horizontal cylinder in a high-porosity non-Darcian regime, *J. Porous Media*, Vol. 12, Issue 6, pp.519-535, 2009.
- [31] Chen S.S. and Leonard R., The axisymmetrical boundary layer for a power-law non-Newtonian fluid on a slender cylinder, *The Chem. Eng. J.*, Vol. 3, pp.88-92, 1972.
- [32] Lin, F. N. and Chen, S. Y, Laminar boundary-layer flow of non-Newtonian fluid, *Int. J. Heat Mass Transfer*, Vol. 22, Issue 10, pp.1323-1329, 1979.
- [33] Pop, I., Kumari, M. and Nath, G., Non-Newtonian boundary layers on a moving cylinder, *Int. J. Eng. Sci.* Vol. 28, Issue 4, pp.303-312, 1990.
- [34] Chang, C.L., Buoyancy and wall conduction effects on forced convection of Micropolar fluid flow along a vertical slender hollow circular cylinder, *Int. J. Heat Mass Transfer*, Vol. 49, Issue 25 – 26, pp.4932–4942, 2006.
- [35] Anwar, I., Amin, N. and Pop, I., Mixed convection boundary layer flow of a viscoelastic fluid over a horizontal circular cylinder, *Int. J. Non-Linear Mechanics*, Vol. 43, Issue 9, pp.814-821, 2008.
- [36] Rehman, M.A. and Nadeem, S., Mixed convection heat transfer in micropolar nanofluid over a vertical slender cylinder, *Chin. Phys. Lett.* Vol. 29, No. 12, 124701, 2012.
- [37] A. J. Chamkha, A.M. Rashad, and A. Aly, Transient natural convection flow of a nanofluid over a vertical cylinder, *Meccanica*, Vol. 48, Issue 1, pp.71-81, 2013.
- [38] Bird RB, Armstrong RC, Hassager O., Dynamics of polymeric liquids. Volume 1: fluid mechanics. Vol 1, 2nd edn. Wiley Interscience, New York, 1987.
- [39] Larson RG, Constitutive equations for polymer melts and solutions, series in chemical engineering. Butterworths, Boston, 1988.

- [40] Truesdell C, Noll W., The non-linear field theories of mechanics. Handbuch der Physik, Band III/3. Springer, Berlin, pp 1–602, 1965.
- [41] R.L. Fosdick, K.R. Rajagopal, Anomalous features in the model of second-order fluids, *Archive for Rational Mechanics and Analysis*, Vol. 70, Issue 2, pp.145-152, 1979.
- [42] J.E. Dunn, K.R. Rajagopal, Fluids of differential type: Critical review and thermodynamic analysis, *Int. J. Eng. Sci.*, Vol. 33, Issue 5, pp.689–729, 1995.
- [43] Gorla, R. S. R., Radiative effect on conjugate forced convection in a laminar wall jet along a flat plate, *Encyclopaedia Fluid Mechanics, Suppl. 3: Advances in Flows Dynamics*, Gulf Publishing, Texas, USA (1993).
- [44] Bég, O. Anwar, J. Zueco, S. K. Ghosh and A. Heidari., Unsteady magnetohydrodynamic heat transfer in a semi-infinite porous medium with thermal radiation flux: analytical and numerical study, *Advances in Numerical Analysis*, Vol. 2011, Article ID. 304124, pp.1-17, 2011.
- [45] H.B. Keller, Numerical methods in boundary-layer theory, *Ann. Rev. Fluid Mech.*, Vol. 10, pp.417-433, 1978.
- [46] M. Kumari, G. Nath., Steady mixed convection stagnation-point flow of upper convected Maxwell fluids with magnetic field, *Int. J. Nonlinear Mechanics* Vol. 44, Issue 10, pp.1048-1055, 2009.
- [47] H-T. Chen, C-K. Chen, Natural convection of a non-Newtonian fluid about a horizontal cylinder and a sphere in a porous medium, *Int. Comm. Heat Mass Transfer*, Vol. 15, Issue 5, pp.605–614, 1988.
- [48] Merkin, J. H., Free convection boundary layer on an isothermal horizontal cylinder, *ASME, Heat Transfer Conference*, paper no.76-HT-16. (1976).
- [49] Nazar, R., Amin, N. and Pop, I., Free convection boundary layer on an isothermal horizontal circular cylinder in a micropolar fluid, *Heat transfer*, Proceeding of the 12th int. conference, 2002.